Catena 198 (2021) 105068

Contents lists available at ScienceDirect

Catena

journal homepage: www.elsevier.com/locate/catena

Hydrodynamic characteristics and evolution law of roll waves in overland flow

Jingwen Wang [a,c], Kuandi Zhang [a,b,*], Pu Li [a], Yu Meng [a], Luyou Zhao [a]

[a] Key Laboratory of Agricultural Soil and Water Engineering of Ministry of Education in Arid Areas, Northwest A&F University, Yangling 712100, China
[b] State Key Laboratory of Soil Erosion and Dryland Farming on the Loess Plateau, Northwest A&F University, Yangling 712100, China
[c] State Key Laboratory of Water Resources and Hydropower Engineering Science, Wuhan University, Hubei 430072, China

ARTICLE INFO

Keywords:
Roll waves
Wave velocity
Wavelength
Overland flow
Critical value

ABSTRACT

The frequent occurrence of roll waves in overland flow can increase the water depth and accelerate sheet erosion. To investigate the variation laws and hydrodynamic characteristics of roll waves, indoor artificial experiments with five roughness types, seventeen flow discharges, and five slope gradients were conducted in a hydraulic flume. The results showed that the evolution process of roll waves is divided into three phases: monochromatic, quasi-sine, and mature wave regions. In addition, the parameter roll-wave velocity increased in terms of its power function with the unit discharges, while the slopes showed that a positive line was related to this increase. An empirical formula of the wave velocity was obtained by conducting a regression analysis after synthesizing the influencing factors. The wavelength varied at a single peak with increasing unit discharges, showing a negative linear correlation with the test slope. Additionally, an empirical formula of the wavelength was derived using regression methods. The correction coefficients in the laminar flow instability zone varied from 0.27 to 0.39, while the Reynolds number was approximately 100. The critical average Freud number Fr and the Onsager value Z were 0.6 and 3.33×10^{-3}, respectively. In addition, the correction coefficients in the turbulent flow instability zone varied within 0.412–0.730, while the Reynolds number fluctuated between 900 and 3300. The range of the critical Fr value was 1.59–2.20, and the critical average Z was 1.88×10^{-3}. These results are vital for understanding the hydrodynamic characteristics and evolution laws of roll waves in overland flow.

1. Introduction

A roll wave is a special type of flow movement that can be widely observed in open channels, debris flows, and shallow flows down an inclined slope (Balmforth and Mandre, 2004; Zhang et al., 2011). Water flow destabilizes and forms a series of waves when hydraulic parameters reach critical values (Yoon and Wenzel, 1971; Emmett, 1978). These waves cause an instantaneous increase in the water flow energy, thus accelerating the sheet erosion (Prasad et al., 2005). In addition, owing to the wave-current coupling phenomenon, the surface velocity of water flow decreases and the bottom velocity increases. This can affect the variation law of shear stress and the dynamic process of sediment incipience and subsidence in sediment-laden flow (Liu et al., 2005). Furthermore, in debris flow, a roll wave containing rocks can cause more damage to humans, animals, and crops on the road (Iverson et al., 2010; Zhao et al., 2015). Additionally, the occurrence of roll waves is undesired by civil engineers because it can periodically increase the water depth, thus causing water to overflow from the channel banks or runoff channels that are designed to accommodate excess flow (Brock, 1969; Di Cristo et al., 2009; Zhao et al., 2015). Therefore, roll waves have practical significance, and it is important to explore their evolution law and analyze their hydrodynamic characteristics (Zhao et al., 2015; Cao et al., 2015).

Some previous studies deduced roll-wave evolution equations in terms of the characteristics of shallow long waves and mathematical theories (Chang et al., 2000; Zanuttigh and Lamberti, 2002; Kranenburg, 2006). However, no consistent conclusions could be drawn owing to limited technical conditions. Brock (1969) studied roll waves in experimental flumes and derived the expressions of wave shape, wave velocity, and wave period by using shallow-water equations. However, no explicit solution of the equation has yet to be found. Using one-dimensional St. Venant equations, Liu et al. (2005) obtained the roll-

* Corresponding author at: Key Laboratory of Agricultural Soil and Water Engineering of Ministry of Education in Arid Areas, Northwest A&F University, Yangling 712100, China; State Key Laboratory of Soil Erosion and Dryland Farming on the Loess Plateau, Northwest A&F University, Yangling 712100, China.
E-mail address: zhangkuandi428@126.com (K. Zhang).

https://doi.org/10.1016/j.catena.2020.105068
Received 25 August 2019; Received in revised form 30 October 2020; Accepted 23 November 2020
Available online 19 December 2020

wave speed and profile and approximately described the characteristics of periodic permanent roll waves. Subsequently, Richardal and Gavrilyukal (2012) and Hu (2015) succeeded in simulating their development process based on Brock's experimental data. However, this method was only applicable to a small part of the actual situation, and thus lacked universality. Fiorot et al. (2015) made considerable progress in measurement methods for ensuring the visualization of roll waves, but large test errors could not be ignored.

The stability of roll waves is highly sensitive to numerous factors, and they are more prone to occurring in overland flow at a shallow water depth and steep slope (Zhao et al., 2015). Bohorquez (2010) stated that minor fluctuations in water depth can improve the stability of the water surface and prevent the occurrence of roll waves. Regarding the effect of flow resistance on roll-wave formation, Zhao et al. (2015) and Meng et al. (2020) confirmed that roll waves do not form in the absence of resistance. However, Longo (2011), Smith et al. (2011), and Wang et al. (2014) emphasized that roll waves are only formed when the flow resistance is within a certain critical value. Therefore, it is apparent that resistance is not conducive to roll-wave formation if it is excessively large or small. Regarding the effect of the underlying surface, Balmforth and Mandre (2004) indicated that the critical Froude number when roll waves occur in a low-amplitude terrain is smaller than when they occur in a large-amplitude terrain, which is consistent with the results obtained by Balmforth and Vakil (2012). This is primarily attributed to the fact that the bottom bed mainly affects the evolution of roll waves through hydraulic transition, and this influence generally occurs downstream of a steep slope (Colombini and Stocchino, 2008).

The critical Froude number has frequently been observed as a criterion for distinguishing the existence of roll waves (Arai et al., 2013; Smith et al., 2011; Thual, 2013). The value of the critical Froude number, Fr, was 0.74 in the laminar instability zone (Julien and Hartley, 1986), which agrees with the result obtained by Ferreira et al. (2015), who stated that it is greater than 0.58. However, for turbulent flows in open channels, at a constant resistance, this value is 2.0 (Armanini and Recchia, 2006). Meanwhile, Chen (1992) found that the critical Froude number is not a definite value and varies with different velocity distributions and hydraulic parameters. The velocity distribution formula is generally considered either exponential or logarithmic. For turbulent flows under hydraulic rough conditions, the critical values with different velocity distributions were found to be 1.589 and 1.623, while for those under smooth conditions, the values were 1.456 and 1.473, which approximated to 1.5, as proposed by Dressler and Pohle (2010). This difference is attributed to the fact that different momentum correction coefficients were selected.

Given the above, it is necessary to study roll waves. Especially in overland flow, this phenomenon is more likely to occur under certain hydraulic conditions because the water depth is generally less than a few millimeters. Roll waves can influence the hydraulics and hydrodynamic force distribution of water flow and accelerate sheet erosion. The current research on roll waves is mainly based on theoretical analysis and numerical simulation. The experimental data are lacking, and thus, the research has substantial limitations. For example, even in some experimental studies (Pan et al., 2009; Zhang et al., 2011; Zhao et al., 2015; Wang et al., 2019b; Meng et al., 2020), roll-wave development has not been specifically described. In addition, these studies were inclined to analyze the effect of experimental or natural conditions on roll-wave parameters, but there are no formulas available for calculating their velocity and wavelength in overland flow. In addition, when studying the critical conditions of roll-wave generation, researchers have mainly focused on laminar instability in overland flow. There are no critical values of the occurrence of turbulence instability when the roll wave reappears. Thus, this study has the following objectives. (1) Describe the roll-wave development characteristics, including waveform and wave coalescence. (2) Discover the relations between the wave parameters and unit discharges as well as the slope gradients, then determine the internal mechanisms and derive a formula for calculating them. (3) Obtain critical values of some parameters, including the Freud number Fr and the Onsager value Z, when roll waves occur in unstable laminar and turbulent flows. These findings aim to explore the hydrodynamic characteristics and evolution laws of roll waves in overland flow and enrich the theories of roll waves on the slope.

2. Materials and methods

2.1. Experimental apparatus

In this study, to control and measure the boundary conditions of overland flow, fixed beds were chosen, which not only ensured that the water flow had no influence on the bed surface but also made it convenient to control the surface roughness. In addition, an artificial water sand cloth was used to make the roughness of the bed surface uniform. Because the water depth of the sheet flow is very shallow, it can be approximated as a two-dimensional flow. Therefore, the evolution process can be investigated by analyzing the hydraulic parameters, such as flow discharge, water depth, and mean velocity. The experimental apparatus comprises a water supplier, lifting system, vortex stabilizer, and test flume, as shown in Fig. 1. Compared to an open-channel flow, the depth of the overland flow is generally less than a few millimeters and the flow direction is unstable. Therefore, the flatness of the test flume directly influences the measured hydraulic parameters, such as water depth and velocity, and ultimately affects the reliability of the test. The test flume has a wide and shallow rectangular section, which is equipped with a supporting structure of section size $50 \times 50 \times 600$ cm^3. The bottom of this flume is covered with a 12-mm-thick plexiglass. The experimental flume area is 6.5 m long, 0.6 m wide, and 0.2 m deep, with a slope range of 0–20°.

2.2. Experimental design

Five different slopes, 3°, 6°, 9°, 12°, and 15°, were used in this experiment, i.e., the slope was designed as $J = 0.0523$, 0.1045, 0.1564, 0.2079, and 0.2588 rad. The following five types of bed conditions were designed: a smooth surface (equivalent roughness = 0.009 mm); a 200- and a 40-mesh gauze bed (particle sizes = 0.245 and 0.380 mm, respectively); and two types of sand-pasted surfaces (particle sizes = 0.750 and 1.500 mm). Moreover, 17 unit discharges (discharge per unit width) were tested according to the experimental objectives and the rainfall intensity in the Loess Plateau region (0.0694, 0.1042, 0.1389, 0.1736, 0.2083, 0.2431, 0.2778, 0.3472, 0.4167, 0.4861, 0.5556, 0.6944, 0.8333, 0.9722, 1.1111, 1.6667, and 2.5 L/(s·m)). There were eight longitudinal cross sections for the observations, positioned at 1.0, 1.5, 2.0, 2.5, 3.0, 3.5, 4.0, and 4.5 m along the slope from top to bottom. For each cross section, five measurement points were set transversely to observe the wave velocity using the $KMnO_4$ dye-tracer and float methods. An SX402 digital probe tester (Chongqing Hydrological Instrument Factory, Chongqing, China) with 0.01-mm precision was used to measure the wave height. The wave period T and wave frequency ω were also visually observed and measured using a digital stopwatch. The travel times of 10 roll waves over each cross section (0.5 m interval from the upslope to downslope) of the flume were recorded with 10 replicates. One roll wave period was obtained by dividing the travel time by 10, and the average of the 10 values was obtained as the mean roll-wave period of a cross section. The roll wavelength was calculated using Eq. (8). When the unit discharge was less than 0.5556 L/(s·m), the volume method was adopted, and when it was greater than 0.5556 L/(s·m), the triangular weir method was adopted. During this experiment, the runoff temperature was also recorded to calculate the kinematic viscosity of the overland flow.

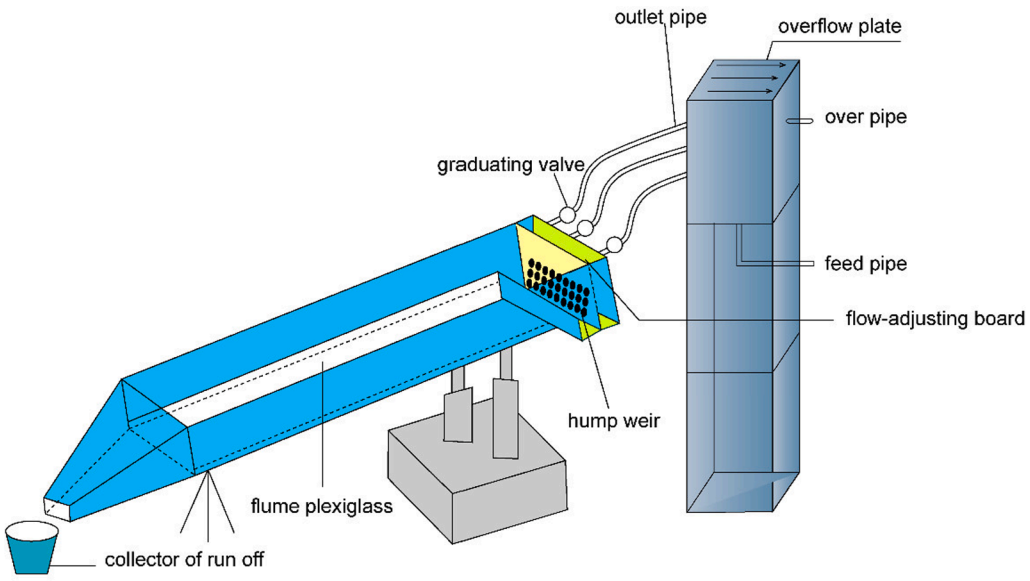

Fig. 1. Schematic of the experimental setup.

2.3. Calculation of hydraulic parameters

(1) Mean velocity of the cross section: According to the continuation equation of water flow, the vertical average velocity u of the overland flow can be calculated as

$$u = \frac{q}{h} \tag{1}$$

where q is the unit discharge (m^2/s) and h is the measured mean water depth (m).

(2) The hydraulic dual-flow Reynolds number can be expressed as

$$Re_h = \frac{uR}{\nu} \tag{2}$$

where R is the hydraulic radius (m) and ν is the viscosity coefficient of the flow (cm^2/s). Compared to the pressure, ν is more sensitive to a varying temperature and, therefore, can be expressed as

$$\nu = 0.01775/\left(1 + 0.337t + 0.000221t^2\right) \tag{3}$$

where t is the temperature of water.

(3) The Froude number can be expressed as

$$Fr = u/\omega \tag{4}$$

where ω is the velocity of the microwave (m/s) and can be expressed as

$$\omega = \sqrt{gh\frac{(1+\Delta h)^2}{\left(1+\frac{\Delta h}{2h}\right)}} \tag{5}$$

where$\Delta h$is the wave height (m) and g is the acceleration due to gravity (9.81 m/s^2).

(4) The Darcy–Weisbach resistance coefficient can be calculated as follows:

$$\lambda = 8gRJ/u^2 \tag{6}$$

Here, the hydraulic gradient J equals sin θ, where θ is the slope gradient.

(5) There are some parameters describing the fluctuation characteristics, including wavelength L, wave velocity C, wave period T, and wave frequency ω, as shown in Fig. 2 (Wang, et al., 2019b). The relationship is:

$$C = L/T \tag{7}$$

Both T and ω represent the vibration intensity of roll waves and have an inversely proportional relation. The wavelength can be calculated as

$$L = CT \tag{8}$$

(6) In mathematical statistics, a comparison between the calculated and measured values can be quantitatively characterized using statistical parameters, such as concentration coefficient, variation coefficient, and standardization error. These three parameters are defined as

$$\text{Concentration factor}: \quad b_p = \frac{1}{n}\sum\frac{C_{0c}}{C_{0t}} \tag{9}$$

$$\text{Variation coefficient}: \quad b_x = \frac{\sum\left|\frac{C_{0c}-C_{0t}}{(C_{0c}+C_{0t})/2}\right|}{n} \tag{10}$$

$$\text{Standardization error}: \quad E_r = \frac{1}{n}\sum_{i=1}^{n}\frac{|C_{0c}-C_{0t}|}{C_{0c}} \tag{11}$$

where C_{0t} is the measured wave velocity and C_{0c} is the calculated wave velocity. The concentration coefficient represents the arithmetic average of the calculated and measured values. The concentration coefficient is close to 1, indicating that the ratio of the calculated to measured values tends to 1:1. The variation coefficient represents the average deviation between the calculated and measured values. When the deviation coefficient approaches zero, it shows that the deviation is negligible. The standardization error, representing the average error of all samples, can be used to measure the computational accuracy of the empirical equations.

2.4. Theoretical analysis

The flow characteristics of roll waves are sensitive to many factors,

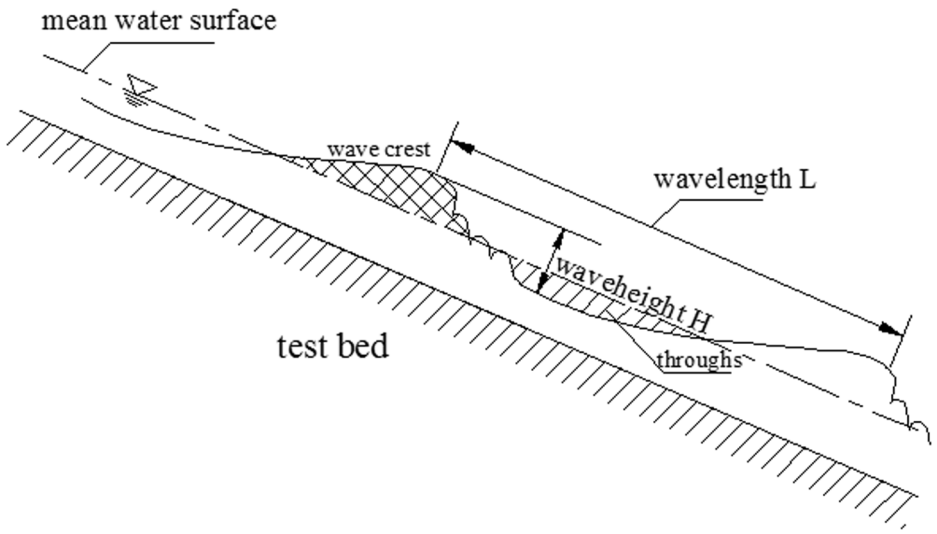

Fig. 2. Geometric parameters of a typical waveform of a roll wave.

which means that flow instability is a common phenomenon in overland flow. Because the ratio of water depth to wavelength is considerably less than 1, the liquid-film flow theory can be used to explore numerous factors that affect the roll-wave movement along steep slopes.

Regarding the evolution equation of liquid films, Ooshida (1999) introduced the "Pade approximation" into the "Benney-type" formula and proposed a standardized equation without traditional long-wave theories. This formula is not only concise but also applicable over a wide range, from the critical Reynolds number to $\mathrm{Re/We}^{1/3} > 1$. It can be expressed as

$$\partial_t h - \frac{4}{21} Re \partial_x \partial_t h^5 - \partial_x (h^2 \partial_x \partial_t h) + \frac{2}{3} \partial_x \left[h^3 - \partial_x \left(\frac{cot\theta}{4} h^4 + \frac{72}{245} Reh^7 \right) + Weh^3 \partial_x^3 h \right] = 0 \tag{12}$$

where θ is the gradient of the bed surface, h is the normalized water-layer thickness without disturbance, x is the coordinate in the water flow direction, and t is the time. The Reynolds number Re and Weber number We can be calculated as

$$Re = \frac{h_{mean} u_{mean}}{\nu} \quad We = \frac{\rho h_{mean} u_{mean}^2}{\sigma} \tag{13}$$

where ν is the viscosity coefficient of the flow, ρ is the water density, and σ is the surface tension coefficient.

The above formula could be expressed using the coordinate transformation approach as follows:

$$\varsigma = x - c_0 t \tag{14}$$

where c_0 is the wave velocity; Eq. (14) shows that

$$\partial_x = \partial_\varsigma \quad \partial_t = -c_0 \partial_\varsigma \tag{15}$$

Eq. (12) can be expressed as Eq. (16) based on $\partial_x = \partial_\varsigma$:

$$C_0 \partial_\varsigma h - \frac{4}{21} C_0 Re \partial_\varsigma^2 h^5 - C_0 \partial_\varsigma (h^2 \partial_\varsigma^2 h) + \frac{2}{3} \partial_\varsigma \left[h^3 - \partial_\varsigma \left(\frac{cot\theta}{4} h^4 + \frac{72}{245} Reh^7 \right) + Weh^3 \partial_\varsigma^3 h \right] = 0 \tag{16}$$

Eq. (17) is established using the integral method and transforming subscripts:

$$C_0 h - \frac{4}{21} C_0 Re \partial_x h^5 - C_0 h^2 \partial_x^2 h) - \frac{2}{3} \left[h^3 - \partial_x \left(\frac{cot\theta}{4} h^4 + \frac{72}{245} Reh^7 \right) + Weh^3 \partial_x^3 h \right] = K \tag{17}$$

Under the boundary conditions,

$$K = C_0 - 2/3 \tag{18}$$

Eq. (17) shows that the evolution process of roll waves is influenced by Re, We, and the slope gradient θ, where Re indicates the effect of inertia force and viscous force, while We represents the influence of surface tension.

3. Results

3.1. Evolution process of roll waves

The evolution process of roll waves, as shown in Fig. 3, included three phases: monochromatic, quasi-sine, and mature wave regions. At a certain distance from the slope crest, the gravity component on the water surface broke down in tangent directions, and disturbance waves appeared. Their vibration along the slope continued to expand and the wave shape gradually became clear. When the disturbance waves developed into monochromatic waves, their amplitudes increased exponentially. For a specific bed at a roughness of 0.380 mm, when the unit discharge was 0.278 L/(s·m), disturbance waves emerged 0.0–100 cm away from the slope crest. These wavelets had a wavelength of approximately 3–5 cm and belonged to the monochromatic wave region. At a distance of 100–200 cm from the slope crest, the amplitude of the monochrome waves gradually increased to approximately 10 cm. This value is closely related to numerous roll waves, unit discharges, slope

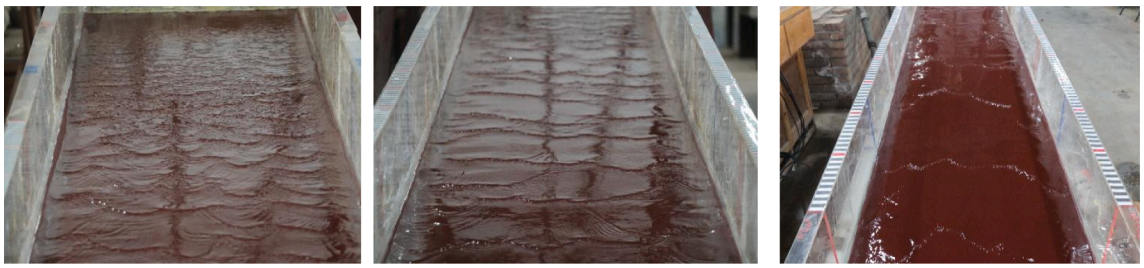

(a) Monochromatic wave region (b) Quasi-sine wave region (c) Mature wave region

Fig. 3. Three phrases of roll-wave evolution.

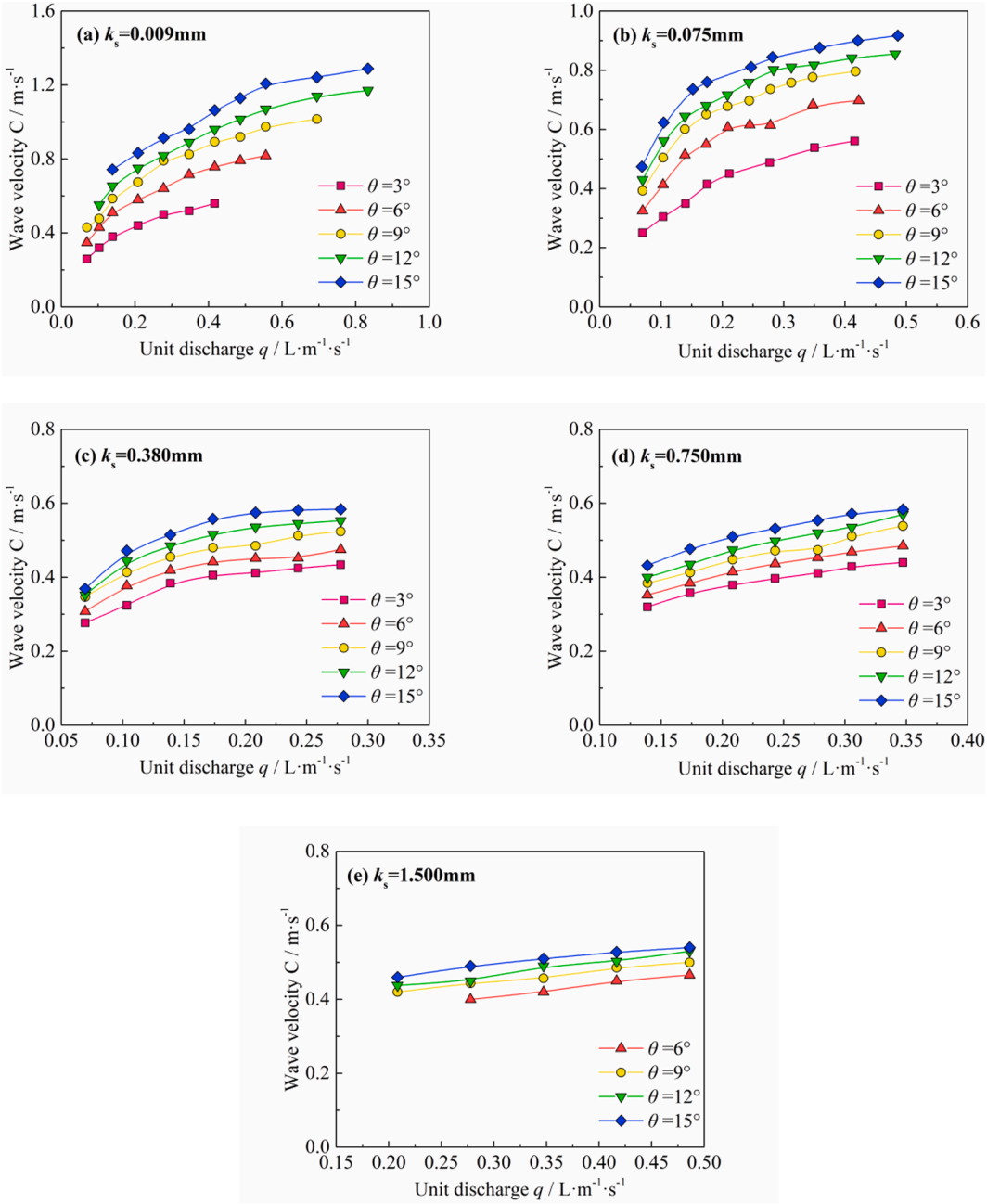

Fig. 4. Relation between the wave velocity and unit discharges.

Table 1
Function relations between the roll-wave velocity and unit discharges with different roughness values on the slope surface.

Bed surface roughness	Slope i	Unit discharge (L/s·m)	Reynolds number	Fitted formulas	Correlation coefficient
0.009	3	0.069–0.417	78–448	$C = 0.834q^{0.422}$	$R^2 = 0.992$
	6	0.070–0.556	73–571	$C = 1.070q^{0.403}$	$R^2 = 0.989$
	9	0.070–0.833	75–824	$C = 1.233q^{0.392}$	$R^2 = 0.986$
	12	0.552–0.833	72–850	$C = 1.299q^{0.359}$	$R^2 = 0.992$
	15	0.743–0.833	72–865	$C = 1.404q^{0.333}$	$R^2 = 0.986$
0.075	3	0.070–0.416	75–440	$C = 0.881q^{0.462}$	$R^2 = 0.984$
	6	0.070–0.422	69–419	$C = 1.081q^{0.417}$	$R^2 = 0.981$
	9	0.070–0.417	69–450	$C = 1.182q^{0.380}$	$R^2 = 0.958$
	12	0.070–0.482	75–533	$C = 1.188q^{0.338}$	$R^2 = 0.982$
	15	0.068–0.486	79–440	$C = 1.219q^{0.310}$	$R^2 = 0.918$
0.380	3	0.073–0.279	78–306	$C = 0.688q^{0.327}$	$R^2 = 0.942$
	6	0.073–0.274	80–300	$C = 0.710q^{0.314}$	$R^2 = 0.924$
	9	0.071–0.279	79–323	$C = 0.772q^{0.298}$	$R^2 = 0.965$
	12	0.068–0.277	73–303	$C = 0.866q^{0.308}$	$R^2 = 0.952$
	15	0.069–0.279	75–299	$C = 0.938q^{0.285}$	$R^2 = 0.968$
0.750	3	0.138–0.347	141–399	$C = 0.6383q^{0.339}$	$R^2 = 0.986$
	6	0.138–0.347	134–404	$C = 0.711q^{0.351}$	$R^2 = 0.990$
	9	0.138–0.352	135–409	$C = 0.777q^{0.358}$	$R^2 = 0.980$
	12	0.138–0.346	134–415	$C = 0.847q^{0.378}$	$R^2 = 0.996$
	15	0.138–0.348	136–408	$C = 0.841q^{0.328}$	$R^2 = 0.985$
1.500	6	0.278–0.486	240–472	$C = 0.572q^{0.283}$	$R^2 = 0.998$
	9	0.208–0.486	180–468	$C = 0.620q^{0.231}$	$R^2 = 0.958$
	12	0.208–0.486	177–457	$C = 0.578q^{0.208}$	$R^2 = 0.987$
	15	0.208–0.486	199–482	$C = 0.622q^{0.198}$	$R^2 = 0.981$

gradients, and Weber number. The finite wave vibration could survive a long distance, which is nearly ten times the disturbance waves' wavelength. This region had relatively stable wave velocity and shape and is called the quasi-sine wave region.

The area beyond 200 cm from the slope crest is called the mature wave region, where the wave shape underwent tremendous variations. The vibrant waves comprised a series of closely connected wave groups, each of which had a roll wave with the largest amplitude. There were several waves with smaller amplitudes in front of them across the entire section, which together formed forward shock waves. The wave velocity did not undergo a significant change and remained stable at approximately 0.3 m/s. Subsequently, the wave shape became more evident, and the wave period increased with the slope length under the substantial roll-wave coalescence.

3.2. Wave velocity

3.2.1. Relation between wave velocity and unit discharges

According to the experimental phenomena, the wave velocity increased with the unit discharges. Fig. 4 illustrates the variation laws between the wave velocity C and unit discharges q.

Fig. 4 shows a power function relation between the roll wave velocity C and flow discharge Q. The wave velocity first increased significantly, and then rose slightly with increasing flow discharges. For example, when the surface roughness k_s was 0.075 mm and the test slope was 3°, the wave velocity increased by 0.099 m/s (0.25–0.349 m/s) as the unit discharge q rose from 0.070 to 0.139 L/(s·m). However, as the unit discharge q rose from 0.350 to 0.416 L/(s·m), it increased by 0.023 m/s (0.538–0.561 m/s), which is 0.232 times higher than that at low discharges. Similarly, when the surface roughness k_s was 0.75 mm and the test slope was 3°, the wave velocity increased by 0.038 m/s (0.32–0.358 m/s) as the unit discharge q rose from 0.139 to 0.174 L/(s·m). However, as the unit discharge q rose from 0.278 to 0.347 L/(s·m), it increased by 0.029 m/s (0.411–0.440 m/s), which is 0.763 times higher than that at low discharges.

Table 1 shows the function relations between the roll-wave velocity and unit discharges under different roughness conditions. Table 1 shows that the roll-wave velocity can be expressed as a power function of unit discharges, and that all determination coefficients are above 0.90. However, the power exponent between C and q varied with surface roughness k_s: As the surface roughness increased, the influence of unit discharges on the wave velocity tended to weaken. A main reason for this is that surface roughness affects the vertical velocity distribution, and therefore, the wave velocity.

3.2.2. Relation between the wave velocity and slope gradient

The slope gradient has always been considered as the main factor affecting the wave velocity on the slope. When the slope increases, the gravity component of water flow increases, thus increasing the wave velocity. Fig. 5 shows the relation between the wave velocity and slope gradient under different roughness conditions.

As shown in the figure, the wave velocity increases in terms of its power function with the slope gradient. At $k_s = 0.009$ and 0.075 mm, this power function relation tends to become more evident, while it seems to be approximately linear at $k_s = 0.750$ and 1.500 mm. This result indicates that under a smooth bed surface, the slope gradient has a strong impact on the wave velocity. However, this influence tends to weaken as the bed roughness increases. For example, when $k_s = 0.009$ mm, the average growth rate of the wave velocity with slopes is 0.0493; when $k_s = 0.075$ mm, the average growth rate is 0.0412; and when $k_s = 1.500$ mm, the growth rate is reduced to a mere 0.0121.

3.2.3. Empirical formula of wave velocity

The roll-wave velocity is mainly influenced by Re, We, and θ. We

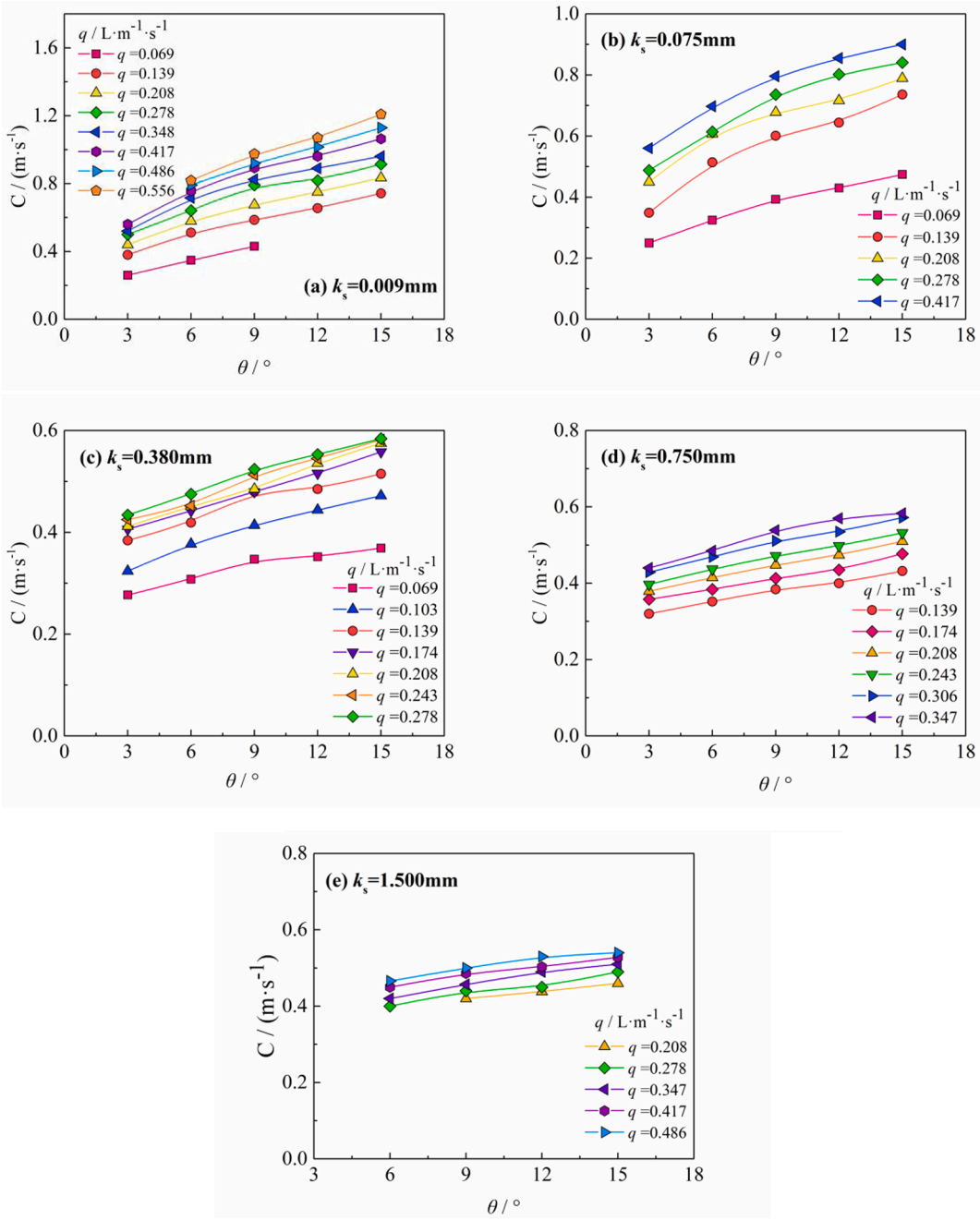

Fig. 5. Relation between the wave velocity and slope gradient.

reflects the inhibitory effect of water flow on roll waves. The combined effects of *Re* and *We* can be expressed using *Z*. Fig. 6 represents the relation between *Z* and *C*.

Fig. 6 shows that the wave velocity decreases linearly with an increasing value of *Z*, but the slope of these straight lines indicates a downward trend as k_s increases. At $k_s = 0.009$ mm, the slope was 3.652, and at 0.075 mm, it was 3.545. Additionally, the slope decreased to 3.212 until k_s reached 1.50 mm. Considering the relations between the wave velocity and Onsager value, as well as the slope gradient, the following empirical formula calculating the wave velocity was derived based on the experimental data:

$$C = -3.47 \times 10^2 Z + 0.018/k_s^{0.25}\theta + 1.356 \quad R^2 = 0.8952 \tag{19}$$

Fig. 7 shows the relation between the measured and calculated values of wave velocity.

The calculated and measured wave velocities are around the 1:1 line ($R^2 = 0.8952$), while some points are scattered around the correlation line. Therefore, this formula can be used to calculate the wave velocity. However, it is relatively complex, and thus, not convenient for direct application in the fields of soil and water conservation. Therefore, a formula requiring a less complex calculation needs to be urgently derived. The variation law of wave velocity is consistent with the mean velocity, and closely related to the bed resistance. According to the formation mechanism of the roll wave, when the resistance of overland flow is not sufficiently large to weaken the undulation of the uneven flow surface, the roll wave occurs (Zhao et al., 2015). Fig. 8 illustrates a logarithmic relation between the dimensionless wave velocity $C_0 = C/u_{mean}$ and resistance coefficient λ.

Fig. 8 shows that the dimensionless wave velocity had a power function relation with the resistance coefficient. Through regression, the

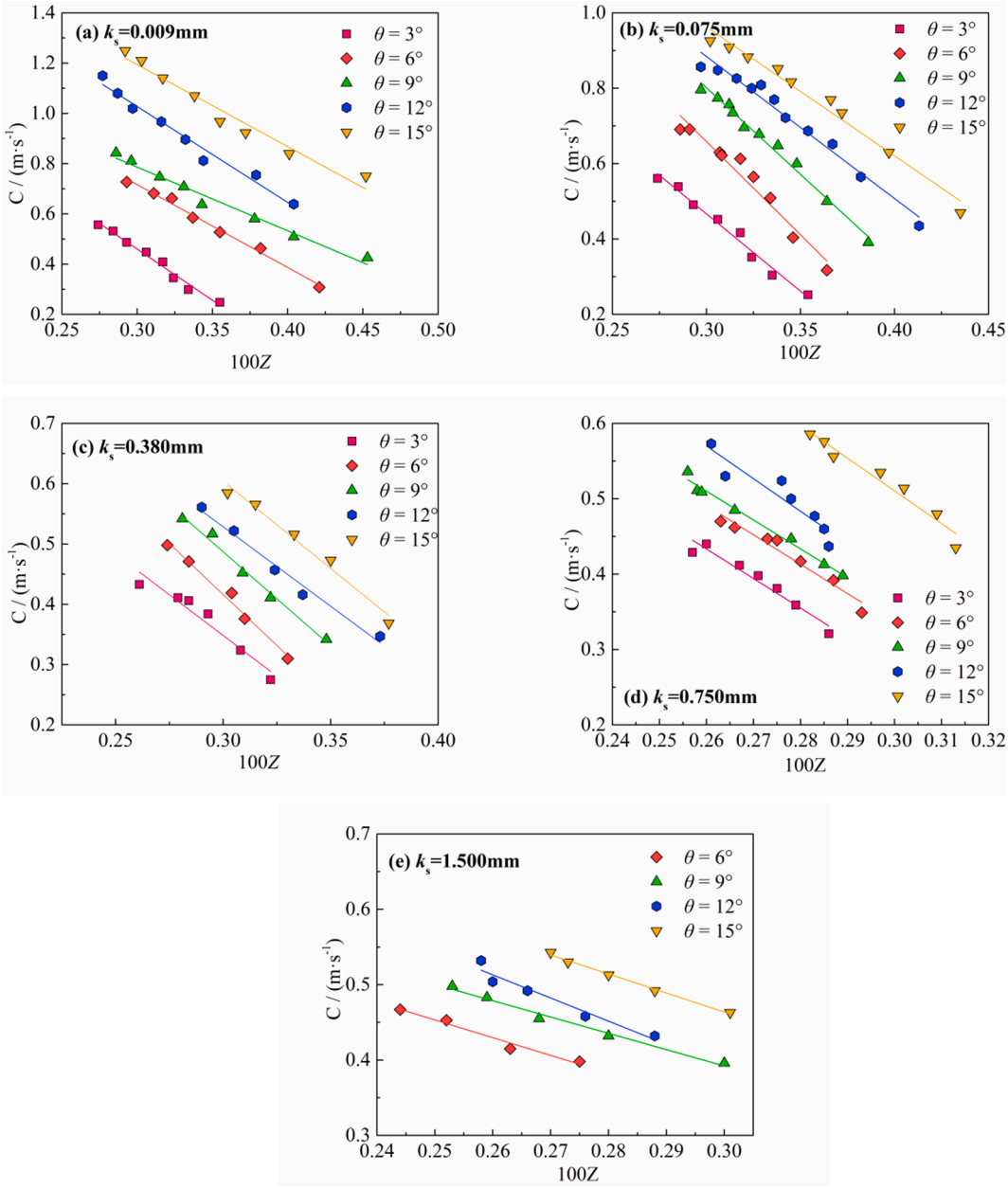

Fig. 6. Relation between the wave velocity and slope gradients.

following formula for calculating the dimensionless wave velocity can be obtained:

$$C_0 = 4.28\lambda^{0.30} \quad R^2 = 0.711 \tag{20}$$

Fig. 9 shows the relation between the measured and calculated values of wave velocity.

According to the figure, the calculated and measured wave velocities are around the 1:1 line ($R^2 = 0.711$). When the wave velocity is between 0.45 and 0.6 m/s, a relatively large error occurs. However, when the wave velocity is above 0.6 m/s, the error seems to be relatively small. The main reason for this is that under this hydraulic condition, roll-wave coalescence in a mature wave region is violent, causing an evident instability of the water flow. Therefore, the wave velocity fluctuates in a wide range, which increases the deviation between the calculated and measured values. With a further increase in the flow intensity, roll waves tend to disappear and the fluctuation is weakened. The wave velocity approaches the mean velocity of the water surface, and thus, the calculated value tends to be close to the measured ones. This trend can also be expressed by statistic parameters, such as concentration coefficient, variation coefficient, and standardization error.

Table 2 shows that the concentration factor b_p was 1.012, approaching 1. The variation coefficient b_x was 0.011 and the standardization error E_r was 0.114. Therefore, Eq. (20) can be used to calculate the wave velocity in overland flow.

3.3. Wavelength

3.3.1. Relation between wavelength and unit discharges

Fig. 10 shows the relations between the wavelength and unit discharges at a specific section (450 cm section).

As shown in the figure, the wavelength increases and then decreases as a single-peak curve with an increasing unit discharge q. For example, when the unit discharge increased from 0.07 to approximately 0.45 L/(s·m), the wavelength first gradually increased and then peaked at a certain value after decreasing gradually. This is attributable to the fact that the average height of the sand particles on the bed is greater than

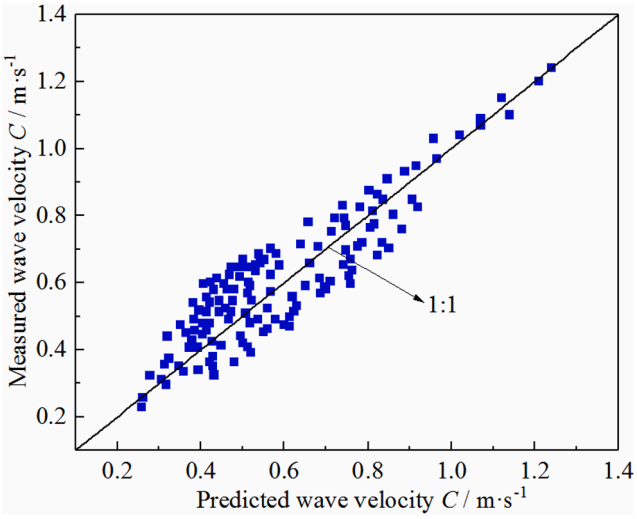

Fig. 7. Relation between the measured and calculated values of wave velocity.

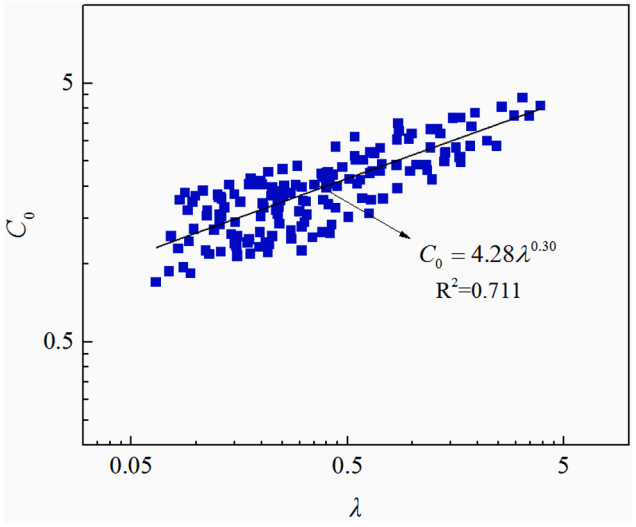

Fig. 8. Relation between C_0 and λ.

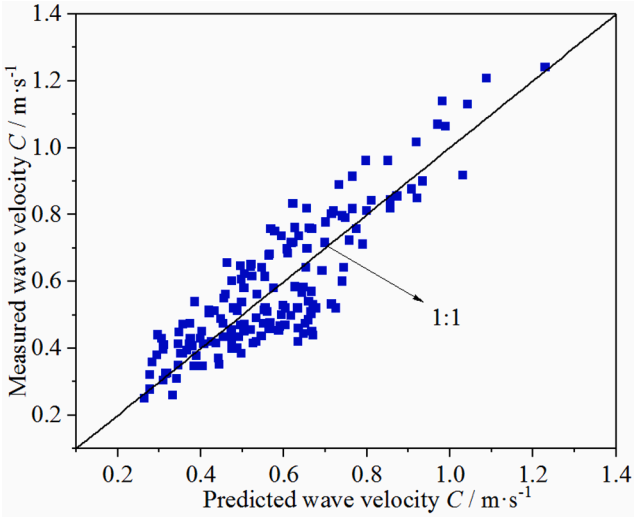

Fig. 9. Comparison between the calculated and measured values of wave velocity.

Table 2
Calculated value of the statistical parameters of Eq. (20).

Eq. (20)	Concentration factor b_p	Variation coefficient b_x	Standardization error E_r
Statistical parameters	1.012	0.011	0.114

the water depth under low flow discharges. As the unit discharge increased, the water flow only moved around the sand particles and a long roll wave was easily formed in overland flow. If the flow discharge was continuously increased to a critical value, the roll waves eventually disappeared in a test flume with limited length. Fig. 10 also shows that the peak value increased with a decreasing slope gradient and reached its maximum at a slope of 3°. At a constant slope gradient, the peak value declined as the bed surface k_s increased and the unit discharge corresponding to it varied. If the curves in Fig. 10 are divided into rising and retreating regions, their corresponding ranges of unit discharges would be considered to be equivalent under low roughness values. As k_s increased, the rising regions tended to become stable, while the retreating regions became steep, and thus, its corresponding ranges of the unit discharges narrowed down.

3.3.2. Relation between the wavelength and slope gradient

Fig. 11 illustrates the relations between the wavelength and slopes under different roughness conditions.

As shown in the figure, there is a negative linear relation between the slope gradient and wavelength L. The wavelength decreased gradually with increasing slope gradient. At the same unit flow discharge, the peak wavelength occurred at the slope of 3° for $k_s = 0.009$, 0.075, 0.380, and 0.750 mm. In contrast, for $k_s = 1.500$ mm, there was no instability on the water surface at 3°, but the roll wave phenomenon occurred when the slope was increased to 6°. These results are consistent with those obtained by Pan et al. (2009), where the wavelength increased with the slope gradient at a slope of less than 3° at flow discharges of 0.208 and 0.422 L/(s·m). However, these researchers did not study the evolution law of roll waves on more gentle slopes. From the perspective of flow balance, it can be inferred that the wavelength is not zero when the slope is zero. Additionally, for a certain flow discharge, the wavelength would be the longest once the flow condition reaches the critical condition of roll-wave occurrence. In addition, the slope of these curves represents the attenuation coefficient of wavelength, which gradually decreases with increasing k_s. For example, when k_s varied from 0.009 to 1.500 mm, the attenuation coefficient decreased from 0.013 to 0.0096. This is mainly because when the resistance is relatively large, it plays an important role in the formation of roll waves compared to the slope gradients. The resistance is large and the water surface flows steadily under a rough surface. Therefore, the variation in wavelength is not evident.

3.3.3. Empirical formula of the wavelength

Overall, the wavelength is closely related to unit discharges and slope gradients. There is a function relation between L_C (the ratio of wavelength and critical length) and Fr, as well as a relative smoothness $d = h/k_s$. Considering the linear relation between L_C and the wavelength $\times$, an empirical formula can be obtained by regression analysis:

$$\frac{L_C}{1000h_k} = 0.02 \ln d\left(\frac{x}{x_w} - 1\right) Fr^{-1/1.5} \quad R^2 = 0.8582 \tag{21}$$

where d is the relative smoothness, x is the length from the slope crest to the test section, and x_w is the initial section forming roll waves.

The variable x_w can be calculated in terms of roll waves in open channels, as follows:

$$\frac{x_w}{1000h_0} = \alpha/\lambda^b \tag{22}$$

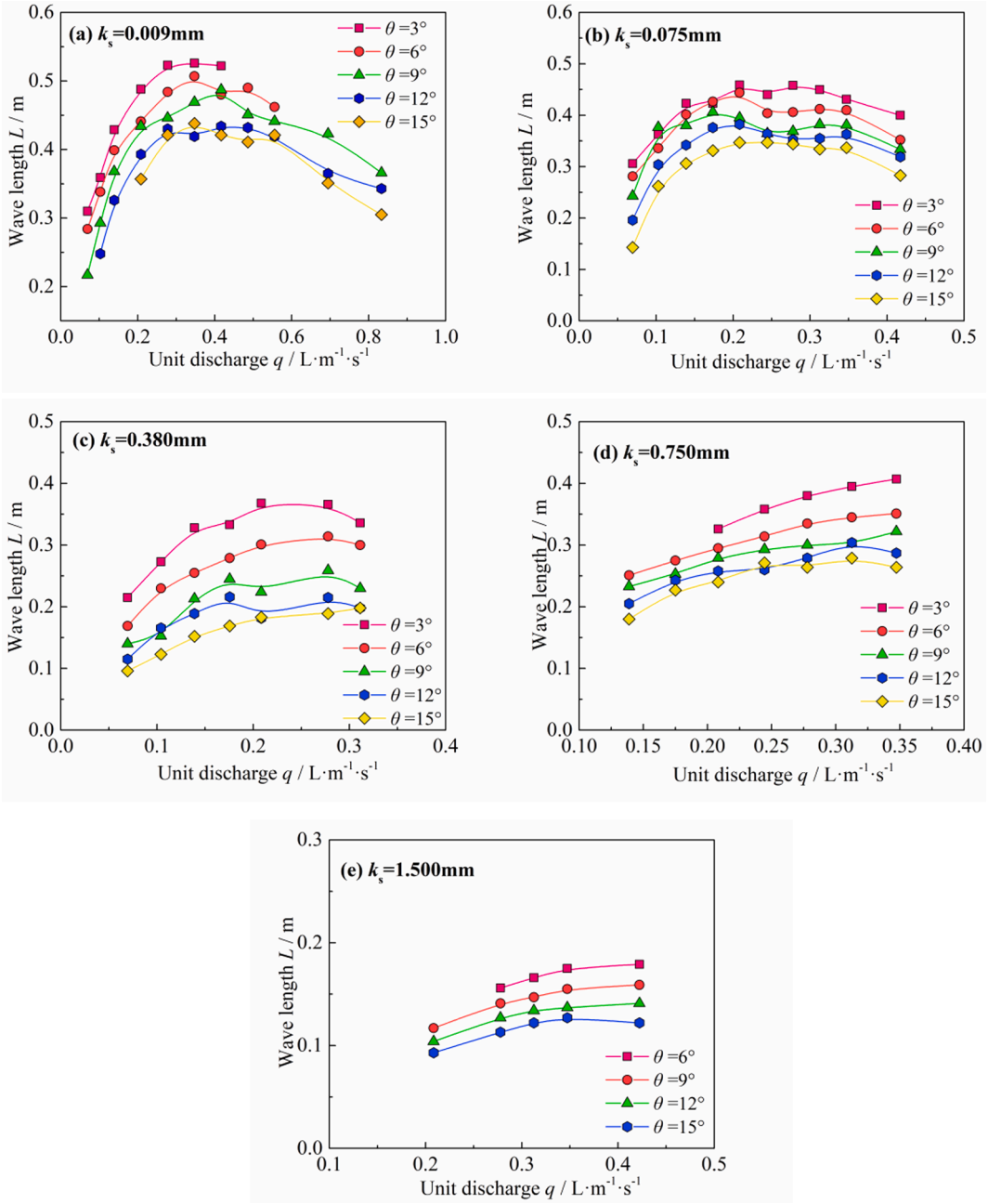

Fig. 10. Relations between the wavelength and unit discharges (450 cm section).

where h_o is the normal water depth in uniform flows and can be approximated as the mean water depth; a is the ratio coefficient, i.e., the comprehensive correction coefficient; and b is the index.

According to characteristic cross-section forming roll waves, x_w in the overland flow can also be expressed based on Eq. (22), where a is 0.5 and b is 1.6:

$$\frac{x_w}{1000h_0} = 0.5/\lambda^{1.6} \tag{23}$$

This expression shows that x_w is proportional to the 1.6th power of the flow resistance coefficient and is inversely proportional to h_o. As h_o is proportional to the 2/3rd power of the flow discharges, it can be concluded that x_w increases with the flow discharges. For a finite test flume, when the flow discharge increases and the resistance coefficient decreases, the x_w value can reach, or even exceed, the entire test length, and thus, the roll waves tend to eventually disappear. To verify the calculation accuracy of Eq. (21), the measured data of 450 cm and 250 cm of a specific section under different roughness conditions were compared with the calculated ones, as shown in Fig. 12. The figure shows that the calculated and measured values are generally scattered around the 1:1 line. It could be argued that this formula can be used to calculate the wavelength in overland flow.

3.3.4. *Critical conditions for surface instability*

Similar to the roll wave in open channels, its occurrence in overland flow may be caused by laminar instability and turbulence instability. As the flow discharge increases gradually, a sequence of roll waves occurs on the slope surface, which flow across the whole section. However, when the flow intensity reaches a certain critical condition, the roll waves disappear and the water surface tends to be stable. If the flow discharge continues to increase, the roll waves would occur again. Regarding the bed with a surface roughness of 0.380 mm, when the

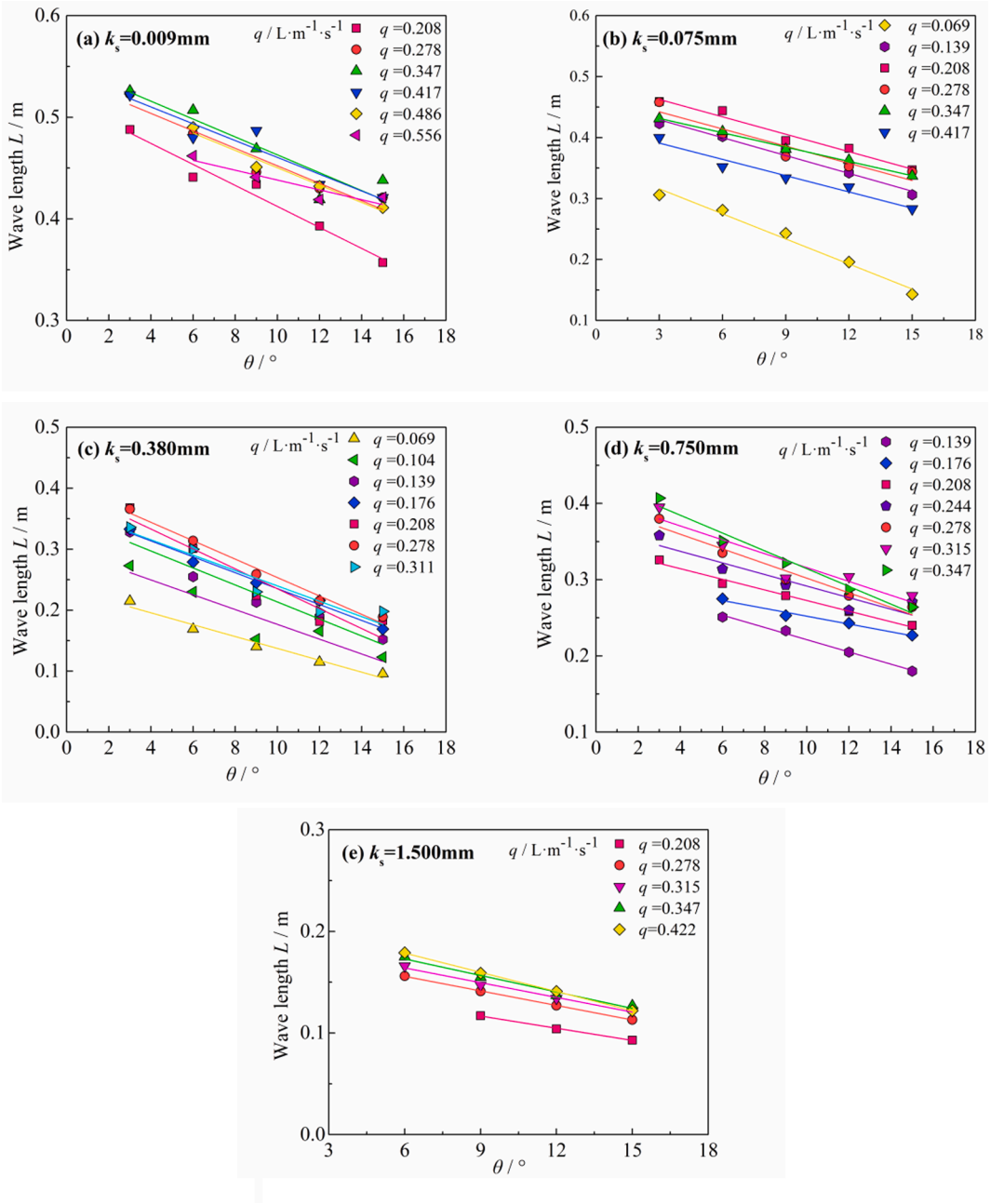

Fig. 11. Relations between wavelength and slope gradient.

slope gradient J was 0.0524 and the unit discharge q was 0.139 L/(s·m), roll waves occurred on the slope surface. In addition, until the value of q was 0.3083 L/(s·m), the roll waves disappeared from the whole section. The Reynolds number under this condition was less than 580, and thus, this instability phenomenon can be considered as laminar flow instability. At a flow discharge larger than 0.9850 L/(s·m), roll waves occurred again. However, their wave forms were disordered and the wave crests were arranged in a tongue shape. This phenomenon is called turbulent instability. As the critical flow discharge in the laminar instability zone is quite small, it is difficult to measure the critical values. Additionally, roll waves are prone to occurring under the conditions of a steep slope. This study only considered the mean hydraulic parameters that correspond to the minimum discharge at 3° slope to explore the variation laws of critical values.

3.3.5. *Critical parameters of the laminar instability zone*

Table 3 shows that the correction factor of velocity is relatively small, ranging from 0.27 to 0.39, and the smoother the bed surface is, the smaller is the value. This association occurs because roll-wave coalescence tends to be more evident under smooth conditions, leading to a smaller ratio of mean velocity to surface velocity. As the surface roughness increases, the velocity distribution becomes uniform, and thus, this correction factor increases. Regarding the flow intensity, the Reynolds number only fluctuated by approximately 100, indicating that the overland flow in this stage is laminar flow. The Freud number varied from 0.5 to 0.7, and the mean critical value was 0.6, approximating to 0.577 by an average cross-section method. This difference is attributable to the measurement errors. This result is approximately consistent with those obtained by Wang et al. (2006) and Zhang et al. (2011); however, Zhang et al. (2011) only considered one experimental surface roughness, 0.38 mm, and therefore, their study lacked rigor. Additionally, the

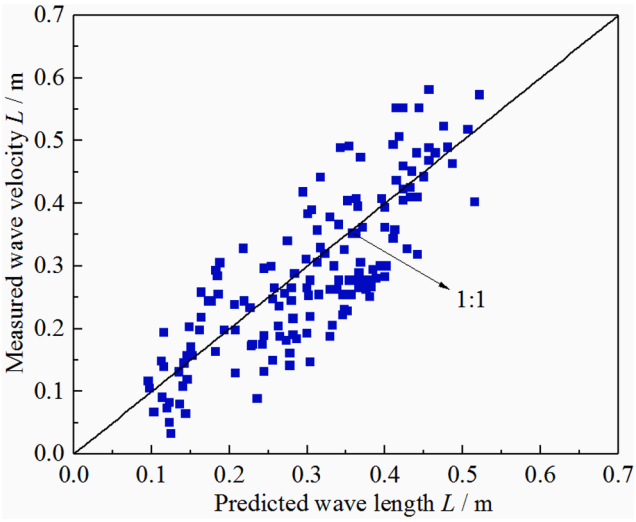

Fig. 12. Comparison between the calculated and measured values of wavelength.

reason for the critical mean value being larger than 0.527 in Wang et al. (2006) is that the roll waves emerged under a flow discharge of less than 0.069 L/(s·m). However, they were not observed under the existing experimental observation conditions. In recent years, Arai et al (2013) and Wang et al. (2014) all agreed with that the Froude number is significant when studying occurrence conditions of roll waves. Wang et al. (2014) found that the roll waves occur at coarse sands rough beds with Fr ranged from 1.61 to 5.24 which is larger than the value in this study. It is mainly because they carried out experiments on steeper slopes. When the roll waves first appeared, the water flow had developed into rapid zones. Apart from this value, Arai et al. (2013) tried to determine critical conditions considering the friction factor. Also Longo (2011) and Smith et al. (2011) proposed that only when the resistance coefficient is less than a critical value, roll waves would occur. This is consistent with my results as in this experimental condition, when roll waves occur, all resistance coefficient is less than nearly 2.5(Table 3 and Table 4). In addition, the Onsager number ranged from 3.0×10^{-3} to 3.9×10^{-3}, with an average value of 3.33×10^{-3}. These values can be seen as the stability criterion in laminar regions of overland flow.

3.3.6. *Critical parameters of turbulent instability zone*

With increasing flow discharge, the velocity and water depth increased, while the inhibition of surface tension decreased substantially. Therefore, an inhibitory effect of the shear force cannot eliminate that of the gravity component, which ultimately makes the water flow enter turbulent regions (i.e., the instability region). Table 3 lists the critical hydraulic parameters of turbulent flow stability under different bed conditions. The roll waves moved upward along the slope and, thus, the critical state here refers to a condition where the roll waves are spread across the entire section.

Table 4 shows that in the turbulent instability zone, the critical flow discharge increased with the surface roughness. For example, it rose from 0.8 to 2.480 L/(s·m) as k_s increased from 0.075 to 2.500 mm. The correction factor of velocity was larger than that in the laminar instability zone, which fluctuated between 0.412 and 0.730. This is mainly because in this region, the velocity distribution was more uniform. Additionally, this value experienced an upward trend with an increase in surface roughness, indicating that rough elements inhibit the roll-wave formation, which is consistent with the roughness theories in a chute spillway. For flow intensity, the Reynolds number varied within 900–3300 and the water flow belonged to a transitional region, according to the traditional discriminant principles. The critical Freud number *Fr* fluctuated between 1.59 and 2.20, which is larger than the theoretical value obtained for overland flow (1.4–1.5). This is because the momentum correction coefficient is 1 in open channels but not applicable to overland flow. The Onsager number varied within 1.35×10^{-3} to 2.22×10^{-3}, with a mean value of 1.88×10^{-3}.

4. Discussion

4.1. *Roll-wave development process*

Through indoor experiments, the roll wave phenomenon can be observed directly, which will help to understand the potential impact of roll waves on slope erosion. As for the evolution phrase, Liu et al. (2005) found two phases of roll-wave development: the initial and final development phases. However, this study divided the roll-wave evolution process into three phases, which is consistent with the results obtained by Di Cristo et al. (2010) and Zhang et al. (2011). Under controlled laboratory conditions, these phases were named monochromatic, quasi-sine, and mature wave regions based on the disturbance wave theory of a thin liquid film. Moreover, similar to the cases of Zanuttigh and Lamberti (2002) and Lu et al. (2008), the roll waves finally began to overtake each other and their frequency decreased. This phenomenon usually occurred at the slope bottom, resulting in energy accumulation and an increase in the flow intensity. Here, the erosion

Table 3
Critical parameters of the laminar instability zone.

Roughness k_s (mm)	Unit discharge (L/s·m)	Water depth (mm)	Surface flow velocity (m/s)	Correction factor of velocity	Reynolds number	Resistance coefficient λ	Froude number	Onsager number Z ($\times 10^{-3}$)
0.075	0.069	1.054	0.242	0.271	75.1	0.977	0.653	3.317
0.024	0.071	1.132	0.185	0.339	63.4	1.176	0.595	3.901
0.038	0.073	1.275	0.165	0.347	77.8	1.575	0.515	3.080
0.750	0.094	1.323	0.241	0.295	92.7	2.372	0.725	3.267
1.500	0.138	1.625	0.217	0.391	117.6	1.850	0.674	3.412

Table 4
Critical parameters of the turbulent instability zone.

Roughness k_s (mm)	Unit discharge (L/s·m)	Water depth (mm)	Surface flow velocity (m/s)	Correction factor of velocity	Reynolds number	Resistance coefficient λ	Froude number	Onsager number Z ($\times 10^{-3}$)
0.075	0.800	2.351	0.826	0.412	869.7	2.20	0.085	2.223
0.245	0.972	3.381	0.658	0.437	1038.7	1.65	0.129	1.886
0.380	1.122	3.665	0.554	0.553	1170.1	1.59	0.167	1.856
0.750	1.440	4.523	0.621	0.513	1398.6	1.62	0.164	1.794
1.500	1.640	5.210	0.614	0.513	1408.1	1.59	0.140	1.891
2.500	2.480	6.324	0.537	0.730	3218.1	1.65	0.161	1.358

transport capacity of the water flow increased. Therefore, the sheet erosion in overland flow gradually developed into gully erosion. At this time, the water depth increased and the cross section became narrow. Accordingly, the hydrodynamic force distribution became nonuniform, causing intense soil erosion. This is why roll-wave characteristics have a possible effect on soil erosion in overland flow.

4.2. Wave velocity variation

This study mainly investigated two wave parameters including wave velocity and wavelength. Among them, the relationship between roll wave velocity and flow discharges, slope gradient and surface roughness was studied in detail. Here, the wave velocity refers to the speed at which the entire waveform of the roll waves moves down the slope. Most of the previous studies have focused on the mean velocity of overland flow, and only a few have considered the effect of roll wave velocity on slope runoff and erosion. This study pointed that, similar to the relation between mean velocity and unit discharges, the wave velocity increases in a power function with increasing discharges. This is similar to the results obtained for a clean water experiment conducted by Yang et al. (2016) and Meng et al. (2020). However, Zhao et al. (2015) proposed that this relation can be described by a linear equation. This difference is attributed to the facts that Zhao et al. (2015). studied wave velocity in sediment-laden flow, the suspended sediment decreased the potential flow erosion, and the influence of roll waves on maintaining the flow stability was not evident. In addition, as the surface wave, the roll-wave velocity in overland flow is always larger than the mean velocity, which was also verified by Zhao et al. (2015) and Natishvili (2016). Zhao et al. (2015) believed that the continuous wave velocity is approximately 1.25 times the mean flow velocity of overland flow, while Natishvili (2016) believed that it is 1.5 times larger than the mean velocity for the cross-sectional wet area.

From a series of formulas and indexes in Table 1, it can be seen more intuitively that as the surface roughness increased, the influence of unit discharges tended to weaken due to variations in the vertical velocity distribution. The flow resistance under comparatively smooth conditions is small and the viscous sublayer is thick, meaning that the mainstream areas account for a small proportion. The vertical velocity distribution is linear, and increases with the unit discharges. However, the water flow is not as turbulent as the open-channel flow and the resistance cannot reach square resistance regions, even under a steady increase in the flow velocity. As the flow discharge increases, the potential energy of water flow increases continuously. The roll waves in overland flow have an “increasing resistance” effect on water flow (Wang et al., 2019a). Thus, to consume more energy and maintain flow instability, the waveform tends to be evident and the wave velocity increases substantially with the unit flow discharges. However, when the surface roughness increases, the viscous sublayer becomes thick and the mainstream areas constitute a substantial proportion. The vertical velocity distribution tends to be exponential and logarithmic, which also increases with the unit discharges. However, the large flow discharge impacts the resistance laws, transforming the proportional relation between resistance and flow discharges into a square relation. In addition, Wang et al. (2019b) drew the waveform and found that with increased roughness, as the rough elements interfere with the water flow, the waveform starts becoming less evident. That is, as the surface roughness consumes more energy provided by the velocity, the roll waves are no longer required to maintain the water flow balance. These inherent mechanisms are consistent with the experimental results obtained by Meng et al. (2020). That is, at a large roughness, the water surface tends to be stable and the wave velocity gradually approaches the mean velocity. Traditionally, the Reynolds number can be expressed as$Re = uh/\nu$. As $uh = q$ in overland flow, $Re = uh/\nu$ can be expressed as$Re = q/\nu$. If the influence of water temperature on the viscosity coefficient is ignored, the unit discharge becomes proportional to the Reynolds number. Thus, the wave velocity also increases with the Reynolds number.

As for the relationship between the wave velocity and slope gradient, the results here agree with those obtained by Zhang et al. (2011), who proposed that, compared to the slope gradient, the unit discharge plays a primary role. As the slope gradient increases, the velocity component along the slope increases, which produces more kinetic energy. Therefore, roll waves are required to maintain the water flow balance, leading to a larger wave velocity. However, the resistance under roughness conditions is larger and can consume more energy; thus, there is no need to rely on roll waves to maintain the balance. At this time, the slope gradient exerts less influence on the wave velocity. Moreover, for the same bed roughness, the gentle slope has a stronger impact on wave velocity compared to steep slopes. This agrees with the conclusions drawn by Zhang et al. (2011) and Yang et al. (2016). The reason for this is attributable to the fact that an increase in the energy slope can prompt potential energies of water flow to transform into kinetic energy, thus increasing the wave velocity. Regarding the steep slopes, the wave velocity increases to a large extent and the resistance reaches the square resistance region. This means that the water surface tends to be stable, and thus, the effect of energy slope on the wave velocity becomes less evident. Generally speaking, the occurance roll wave is a way of energy consumption, and the wave velocity is greatly influenced by external conditions.

4.3. Calculation formulas for wave parameters

At present, there are few formulas to calculate the wave velocity and wavelength of roll waves on the slope. In this study, there are two formulas derived for the wave velocity. From the above, Eqs. (19) and (20) can be used to calculate the roll wave velocity, where the former is derived from the influencing factors of roll waves, while the latter is derived from its formation mechanisms. Previously, Liu et al. (2005) found that the roll wave velocity can be mainly calculated from the resistance coefficient, cosine value of slopes, slope gradient under the critical condition, and mean flow depth in one wavelength. Here, the critical condition indicates that the flow turns from the relative subcritical flow into the relative supercritical flow in one wavelength. The viscous force and surface tension restrain the roll-wave formation, while the inertial force mainly destroys the flow stability and induces roll waves. Compared to Eqs. (19) and (20), the roll-wave velocity calculation proposed by Liu et al. (2005) also considered the effects of the slope, resistance coefficient, inertial force, and viscous force. However, owing to the limitation of the measurement technology, it was difficult to distinguish the critical condition. In addition, it ignores the influence of surface tension, and thus, may be less accurate and applicable than Eqs. (19) and (20) in this study.

In addition, as the wavelength is sensitive to numerous factors, the computation accuracy of these empirical formulas is not satisfactory. There are two reasons that can account for this result. (1) The wavelength was calculated using the wave velocity and wave period, and thus, their computation error had a strong impact on the formula. (2) Under a fixed flow discharge, nearly all hydraulic parameters substantially influence the roll wavelength (Zhao et al., 2015), and thus, it is difficult to discover a high-precision formula. Therefore, it is necessary to improve the measurement technology of these basic hydraulic parameters in the future, and hopefully obtain better experimental rules.

5. Conclusions

The occurrence of roll waves in overland flow substantially impacts the development of sheet erosion on the slope. Through simulated roughness tests, this study systematically depicted the experimental phenomenon and investigated the evolution characteristics, parameter variation, and critical values of flow instability. According to the results, the evolution process of roll waves included monochromatic, quasi-sine, and mature wave regions. Both the roll-wave velocity and wavelength

are important parameters in overland flow, and their relations with unit discharges and slope gradient were thoroughly studied. Subsequently, considering the influencing factors, formulas for calculating both the roll-wave velocity and wavelength were derived. In addition, through the experimental phenomenon, some critical values, such as the correction factor, Reynolds number, resistance coefficient, Froude number, and Onsager number, were obtained in the laminar and turbulent flow instability zones.

Unlike most studies conducted on roll waves, this study focused on overland flow and conducted laboratory experiments. In addition, the results and analysis were based on the experimental phenomenon and mechanisms of roll-wave generation. It is vital to completely understand the essence of suspended sediment transport in overland flow. In addition, the two formulas and critical values should be considered in sheet erosion models to improve the prediction accuracy, especially on slopes where flow instability and roll waves occur.

Data availability

All data used during the study are available from the corresponding author on request.

Declaration of Competing Interest

The authors declare that they have no known competing financial interests or personal relationships that could have appeared to influence the work reported in this paper.

Acknowledgements

This research was supported financially by the National Natural Science Foundation of China [Grant No. 51579214, 41877076], Fundamental Research Business Expenses of Central Universities [2452017321].

References

Armanini, A., Recchia, N., 2006. Experimental analysis of roll waves in overconcentrated flow. In: Proceedings of the INTERPRAEVENT International Symposium Disaster Mitigation of Debris Flows, Slope Failures and Landslides, Niigata. Japan, pp. 149–157.
Arai, M., Huebl, J., Kaitna, R., 2013. Occurrence conditions of roll waves for three grain fluid models and comparison with results from experiments and field observation. Geophys. J. Int. 195, 1464–1480.
Balmforth, N.J., Mandre, S., 2004. Dynamics of roll waves. J. Fluid. Mech. 514, 1–33.
Balmforth, N.J., Vakil, A., 2012. Cyclic steps and roll waves in shallow water flow over an erodible bed. J. Fluid. Mech. 695 (3), 35–62.
Bohorquez, P., 2010. Competition between kinematic and dynamic waves in floods on steep slopes. J. Fluid. Mech. 645 (6), 375–409.
Brock, R.R., 1969. Development of roll-wave trains in open channels. J. Hydraul. Div. 95, 1401–1428.
Cao, Z.X., Hu, P.H., Hu, K.H., Gareth, P., Liu, Q.Q., 2015. Modelling roll waves with shallow water equations and turbulent closure. J. Hydraul. Res. 53 (2), 161–177.
Chang, H.C., Demekhin, A., Kalaidin, E., 2000. Coherent structures, self-similarity, and universal roll wave coarsening dynamics. Phys. Fluids 12 (9), 2268–2278.
Chen, C.L., 1992. Unique laminar-flow stability limit based on shallow-water theory. J. Hydraul. Eng. 119 (7), 816–829.
Colombini, M., Stocchino, A., 2008. Finite-amplitude river dunes. J. Fluid. Mech. 611 (611), 283–306.
Di Cristo, C., Iervolino, M., Vacca, A., Zanuttigh, B., 2009. Roll-waves prediction in dense granular flows. J. Hydrol. 377, 50–58.
Di Cristo, C., Iervolino, M., Vacca, A., Zanuttigh, B., 2010. Influence of relative roughness and Reynolds number on the roll-waves spatial evolution. J. Hydraul. Eng. 136, 24–33.
Dressler, R.F., Pohle, F.V., 2010. Resistance effects on hydraulic instability. Commun. Pur. Appl. Math. 6 (1), 93–96.
Emmett, W.W., 1978. In: Overland flow. Hillslope hydrology. Wiley, New York, pp. 145–175.
Ferreira, F.d.O., Maciel, G.d.F., Fiorot, G.H., Cunha, E.F.d., 2015. Natural hazards modeling: from runoff to hyperconcentrated flows -roll waves generation. IACSIT Int. J. Eng. Technol. 7, 204-208.
Fiorot, G.H., Maciel, G.F., Cunha, E.F., Kitano, C., 2015. Experimental setup for measuring roll waves on laminar open channel flows. Flow. Meas. Instrum. 41, 149–157.
Hu, P., 2015. Modelling roll waves with shallow water equations and turbulent closure. J. Hydraul. Res. 53 (2), 161–177.
Julien, P.Y., Hartley, D.M., 1986. Formation of roll waves in laminar sheet flow. J. Hydraul. Res. 24 (1), 5–17.
Iverson, R.M., Logan, M., LaHusen, R.G., Berti, M., 2010. The perfect debris flow Aggregated results from 28 large-scale experiments. J. Geophys. Res. 115, F03005.
Kranenburg, C., 2006. On the evolution of roll waves. J. Fluid. Mech. 245 (245), 249–261.
Liu, Q.Q., Chen, L., Li, J.C., Singh, V.P., 2005. Roll waves in overland flow. J. Hydrol. Eng. 10, 110–117.
Longo, S., 2011. Roll waves on a shallow layer of a dilatant fluid. Eur. J. Mech. B. Fluids 30, 57–67.
Lu, C., Duan, R.Q., Jiang, S.Y., 2008. Experimental study of flow instabilities of falling films. J. Tsinghua. Univ. (Sci. & Tech.) 48 (9).
Meng, H., Wang, J.W., Zhang, K.D., 2020. Influence factors of hydraulic parameters of roll waves in overland flow. Adv.water. sci. 31 (1), 102–111 (in Chinese with English abstract).
Natishvili, O.G., 2016. On the problem of velocity of long continuous waves in overland flows. Russ. Meteorol. Hydro. 41 (1), 72–75.
Ooshida, T., 1999. Surface equation of falling film flows with moderate Reynolds number and large but finite Weber number. Phys. Fluids. 11, 3247–3269.
Pan, C.Z., Shangguan, Z.P., Experimental study on influence of rainfall and slope gradient on overland shallow flow hydraulics. J. Basic. Sci.Eng. 17(6), 843-851 (in Chinese).
Prasad, S.N., Rao, S.M., Romkens, M.J.M., 2005. Experimental Observations of the Effect of Particle Interactions on the Transport Capacity in Shallow Overland Flow.
Richardal, G.L., Gavrilyukal, S.L., 2012. A new model of roll waves: comparison with Brock's experiments. J. Fluid. Mech. 698, 374–405.
Smith, M.W., Cox, N.J., Bracken, L.J., 2011. Modeling depth distributions of overland flows. Geomorphology 125, 402–413.
Thual, O., 2013. Modelling rollers for shallow water flows. J. Fluid. Mech. 728, 1–4.
Wang, J.W., Zhang, K.D., Yang, M.Y., Meng, H., Li, P., 2019a. The effect of roughness and rainfall on hydrodynamic properties of overland flow. Hydro. Res. 50 (10), 1324–1343.
Wang, J.W., Lv, X.R., Zhang, K.D., Li, P., Meng, H., 2019b. Unsteady-state hydraulic characteristics of overland flow. J. Hydrol. Eng. 24 (10), 04019046.
Wang, X.K., Yan, X.F., Zhou, S.F., Huang, E., Liu, X.N., 2014. Longitudinal variations of hydraulic characteristics of overland flow with different roughness. J. Hydrodyn. 26, 66–74.
Wang, Y.H., Yu, G.H., Hu, Y.J., 2006. Instabilities of free surface in open-channel flows and development of roll waves. Adv. Water. Sci. 17(6), 49–54, 881–886 (in Chinese with English abstract).
Yang, M., Zhang, K.D., Yang, M.Y., Gong, J.G., Zhao, Y., Wang, H., Fan, D., 2016. Expriemnt on evolution law of thin layer rolling flow on slope surface. T. Chin. Soc. Agric. Mach. 47(010), 156-163 (in Chinese with English abstract).
Yoon, Y.N., Wenzel, H.G., 1971. Mechanics of sheet flow under simulated rainfall. J. Hydraul. Div. 97 (9), 1367–1386.
Zanuttigh, B., Lamberti, A., 2002. Roll waves simulation using shallow water equations and weighted average flux method. J. Hydraul. Res. 40, 610–622.
Zhao, C., Gao, J., Zhang, M., Zhang, T., Wang, F., 2015. Response of roll wave to suspended load and hydraulics of overland flow on steep slope. Catena 133, 394–402.
Zhang, K.D., Wang, G.Q., Wang, Z.L., Liu, J.E., Lv, H.X., 2011. Experiments on hydraulic characteristics of roll wave for sheet flow with artificial rough bed. Trans. CSAE 27 (4), 28–34 (in Chinese with English abstract).